Control Engineering Practice 173 (2026) 106936

Contents lists available at ScienceDirect

Control Engineering Practice

journal homepage: www.elsevier.com/locate/conengprac

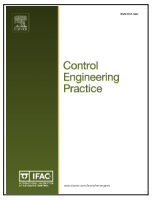

Robust vessel maneuvering modelling using set-membership identification ⋆

Abhishek Dhyani [a,*], Anastasios Tsolakis [a], Kasper van der El [b], Rudy R. Negenborn [a], Vasso Reppa [a]

[a] Department of Maritime and Transport Technology, Delft University of Technology, the Netherlands
[b] Damen Research Development and Innovation B.V., the Netherlands

ARTICLE INFO

Keywords:
Ship manoeuvring
System identification for marine systems
Maritime transport operation and automation
Autonomous marine systems and vehicles

ABSTRACT

System identification of full-scale surface vessels must address significant uncertainties arising from model mismatch, sensor noise, and environmental disturbances. To provide safety, robustness, and constraint satisfaction guarantees, especially for autonomous navigation applications, it is essential to quantify the bounds of parametric model uncertainty. This paper proposes a set-membership identification method for estimating key parameters of a nonlinear vessel maneuvering model, including inertia and added-mass terms, other hydrodynamic derivatives in the Coriolis-centripetal, damping matrices, and actuation-related parameters. The method provides a bounded-error characterisation of uncertainties, offering a reliable framework for modelling the effects of measurement noise, wind, and waves. It involves computing a data-driven parameter set (DDPS) using input-output measurements and model assumptions, which is further used to compute a feasible parameter set (FPS). The parameter estimates are then obtained by iteratively solving a quadratic program over the FPS polytope. Validation of the method using experimental data from a full-scale catamaran demonstrates improved accuracy of up to 26.5% as compared to existing approaches, significantly faster computational times, and its capability to provide bounded parameter estimates.

1. Introduction

Accurate prediction of ship maneuvering motions is essential for safe and efficient autonomous operations, particularly in confined waterways such as rivers, canals and port areas. To obtain accurate maneuvering models, a combination of model-scale free-running experiments (using a scaled model of the vessel) and mathematical model-based methods is often employed (Alexandersson et al., 2022). Free-running experiments, including turning circles, zig-zag and spiral maneuvers, provide realistic measurements of the vessel behaviour in environments such as towing tanks, lakes or open seas. Based on these experiments, model-based system identification methods estimate key physical parameters of the vessel, including the hydrodynamic coefficients. The resulting models facilitate precise predictions of the vessel's maneuvering performance, making them suitable for applications such as autopilot control design, route planning, collision avoidance and fault diagnosis algorithms (Dhyani et al., 2026, 2025; Zhang et al., 2025).

Model-scale tests and simulations require extrapolation to full scale (conforming to the vessel's actual size), which introduces significant uncertainties from scale effects and environmental variations (Birk, 2019). As a result, further validation using full-scale experiments is necessary. For vessels already in service, such tests are typically preferred for system identification. However, identification from full-scale data must particularly address significant modelling and measurement uncertainties (Alexandersson et al., 2022). Moreover, some parameters are inherently challenging to identify due to their dependence on specific operations and environmental conditions. In particular, multicollinearity among hydrodynamic terms can make strongly correlated coefficients difficult to distinguish and accurately identify (Luo, 2016).

Recent studies have explored a range of data-driven and model-based approaches for full-scale vessel identification (see Table 1). In Wang et al. (2024), a neural-network model with multistep constraints was used to capture the dynamics of a full-scale offshore research vessel. Zhang et al. (2022) employed a support vector regression method

⋆ The research leading to these results has received funding from the European Union's Horizon 2020 and Horizon Europe research and innovation programmes under the Marie Skłodowska-Curie grant agreement No 955768 (MSCA-ETN AUTOBarge), and the grant agreement No 101202581 (WARRANT project). This publication reflects only the authors' view, exempting the European Union and the European Climate, Infrastructure and Environment Executive Agency (CINEA) from any liability.

* Corresponding author.
E-mail addresses: a.dhyani-1@tudelft.nl (A. Dhyani), a.tsolakis@tudelft.nl (A. Tsolakis), kasper.van.der.el@damen.com (K. van der El), r.r.negenborn@tudelft.nl (R.R. Negenborn), v.reppa@tudelft.nl (V. Reppa).

https://doi.org/10.1016/j.conengprac.2026.106936
Received 1 November 2025; Received in revised form 12 March 2026; Accepted 12 March 2026
Available online 3 April 2026

combined with a modified grey wolf optimiser for predicting the states of the full-scale vessel *Yukun*. Although these methods achieve good predictive performance, they are purely data-driven and yield parameters that lack physical interpretability, limiting their usefulness for physics-based modelling and control design. To address this limitation, Wang et al. (2022) proposed a hybrid approach that combines a known vessel model with a neural network-based calibrator. However, the procedure for identifying the physical model parameters remains unspecified. Alternatively, several studies have adopted white-box or grey-box modelling approaches to preserve the link to the physical parameters. For instance, Pedersen (2019) applied grey-box identification to identify a simplified model of the fully-actuated ferry *MilliAmpere*. Sonnenburg and Woolsey (2013) applied the least squares method to identify a set of linear first-order models, including a Nomoto (steering) model, a sideslip lag model, a speed model, and a bilinear thruster model for a rigid hull inflatable vessel *Ribcraft*. In Eriksen and Breivik (2017), the identification of a simple two degrees-of-freedom (DOF) model for an agile leisure boat *Telemetron* was carried out using linear regression and full-scale identification experiments. Wu et al. (2022) employs a support vector regression algorithm to identify the linear and nonlinear hydrodynamic coefficients as well as the damping coefficients of pitch and roll motions through sea trials and simulations. Song et al. (2022) proposed a multi-innovation least squares algorithm to identify the 4-DOF vessel dynamics, and demonstrated its application to full-scale trial data from the *Yukun* training ship. Revestido Herrero and Velasco González (2012) presented an unscented Kalman filtering approach for parameter identification of marine vessels, and applied it to identify the parameters of a high-speed trimaran ferry. Hahn et al. (2023) presented an estimation approach that was employed for the identification of a full-scale tugboat using measurement data from regular operation. Zhang et al. (2024) performed experimental identification of the decoupled dynamics of a catamaran ferry, focusing on the surge and yaw motions using a bounded nonlinear least squares algorithm. Most existing full-scale identification studies either focus on simplified or decoupled system dynamics or estimate only a few parameters. Only a few works, such as Revestido Herrero and Velasco González (2012), Song et al. (2022), consider the complete nonlinear dynamics.

Epistemic uncertainties arising from imperfectly known system parameters and initial conditions can significantly affect identification performance, thereby necessitating robustness considerations in the identification process (Der Kiureghian & Ditlevsen, 2009). Conventional identification methods, such as stochastic approaches, provide a probabilistic treatment of uncertainties; however, the identified parameters often remain statistically unbounded, especially in nonlinear settings. This can reduce confidence in the obtained estimates, as the optimisation may converge to local minima. Furthermore, the assumptions about the distributions of random variables (e.g., Gaussian with known mean and standard deviation) are often strict.

In contrast to this approach, a bounded-error characterisation of uncertainties, while more conservative, avoids assumptions related to the noise distribution model and the independence of the underlying random variables. The set-membership identification (SMI) framework utilises this principle to compute parameter sets consistent with the data and the assumed uncertainty bounds, such as the measurement noise and external disturbances (Milanese & Vicino, 1991). Consequently, SMI provides not only the nominal parameter estimates but also bounds that enclose the true parameters. This formulation supports robust prediction and control design, ensuring the model's validity within explicitly defined uncertainty sets. Furthermore, online identification/update of the system parameters and states facilitates real-time gain scheduling, state estimation and fault detection (Rauh et al., 2023). Applying SMI to full-scale vessel system identification becomes particularly attractive, as it can further facilitate adaptive and robust control design, ensuring safe operation under uncertain or variable operating conditions (Lorenzen et al., 2019; Tanaskovic et al., 2014).

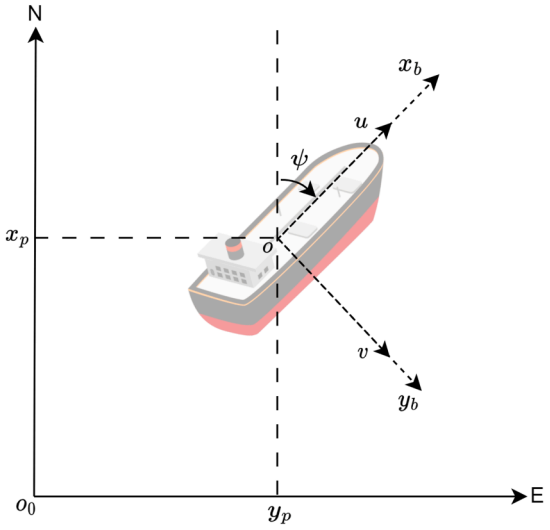

Fig. 1. The coordinate system of a surface vessel. The variables (x_p, y_p) represent the coordinates of the vessel's position in the o_0 frame. u, v and ψ are the surge, sway velocities and the heading angle, respectively (Figure adopted from Dhyani et al., 2026).

This work presents a systematic approach for system identification of a full-scale, three-degrees-of-freedom (3-DOF) vessel model using the SMI method. Unlike existing approaches that yield unbounded parameter estimates, the proposed framework explicitly accounts for unknown but bounded sensor noise and external disturbances affecting the vessel's measured states, thereby enabling robust parameter estimation. The identification problem is formulated as a quadratic program (QP), which reduces to a convex linear optimisation problem, ensuring computational efficiency and convergence. To the best of the authors' knowledge, parameter identification of a full-scale catamaran-type vessel using this framework has not been reported in the literature. Therefore, this work also demonstrates the practical application of the SMI method to real-world experimental data, establishing its effectiveness for full-scale identification under realistic operating conditions.

The remainder of the paper is organised as follows: In Section 2, the vessel's nonlinear maneuvering model and thrusters model are introduced, along with the key parameters to be identified. Section 3 provides a detailed description of the proposed SMI method, which involves computing the feasible parameter set (FPS) that is guaranteed to include the true parameters. In Section 4, the proposed method is validated through parameter identification of a catamaran-type passenger ferry (DAMEN Waterbus 2907) by utilising logged data from multiple maneuvers performed during river trials. The method yields both optimal point estimates and bounded parameter sets, providing robust uncertainty quantification. Validation using synthetic data is performed to benchmark the algorithm's performance under idealised conditions. Additionally, sensitivity analysis is performed to determine the most crucial parameters for accurate identification. Finally, in Section 5, the conclusions and key findings are summarised.

2. Vessel maneuvering model

Fig. 1 illustrates the coordinate system of a vessel in 3-DOF with the North-East-Down reference frame ($o_0 - NED$) and the body-fixed reference frame ($o - x_b y_b z_b$) (the D- and z_b-axes are not shown). Its detailed kinetic and kinematic model are described in the following subsections.

2.1. 3-Degrees of freedom (DOF) maneuvering model

The 3-DOF dynamical model of the vessel can be expressed by

Table 1
Categorisation of studies on full-scale vessel identification.

Reference	Vessel and Type	Identification Method	Model Identified	Model Accuracy	Computational Complexity
Revestido Herrero and Velasco González (2012)	Trimaran ferry	Nonlinear prediction error method, Unscented Kalman filter	4-DOF model (including roll dynamics)	Moderate-High	High
Sonnenburg and Woolsey (2013)	Ribcraft, Inflatable boat	Least squares method	First-order speed and yaw-rate models	Moderate-High	Low
Eriksen and Breivik (2017)	Telemetron, Leisure boat	Linear regression	First-order speed and yaw-rate models	Moderate-High	Low
Pedersen (2019)	MilliAmpere, Ferry	Grey-box modelling	3-DOF fully-coupled and surge-decoupled models	Moderate-High	Moderate-High
Hahn et al. (2021, 2023)	Multratug 32, Tugboat	Model-based estimation	Linear 3-DOF model	Moderate-High	Low
Zhang et al. (2022)	Yukun, Training Ship	Support vector regression, Modified grey wolf optimiser	3-DOF black-box model	High	High
Song et al. (2022)	Yukun, Training Ship	Multi-innovation least squares method	4-DOF model (including roll dynamics)	Moderate-High	Moderate
Wu et al. (2022)	Inflatable boat	Support vector regression	3-DOF model	Moderate-High	Moderate
Wang et al. (2022)	Gunnerus, Research vessel	Hybrid neural network model	3-DOF hybrid model	High	High
Wang et al. (2024)	Gunnerus, Research vessel	Neural network with multistep constraints	3-DOF black-box model	High	High
Zhang et al. (2024)	Maverick, Catamaran	Nonlinear least squares method	Decoupled surge and yaw-rate models	Moderate-High	Moderate
This paper	**Waterbus 2907, Catamaran**	**Set-membership identification**	**3-DOF model**	**High**	**Low**

$$\dot{\eta} = R(\psi)\nu, \tag{1a}$$
$$M\dot{\nu} + C(\nu)\nu + D(\nu)\nu = \tau + \tau_d, \tag{1b}$$

where $\eta = \begin{bmatrix} x_p & y_p & \psi \end{bmatrix}^T$ is the generalised coordinate vector in the NED frame, and $\nu = \begin{bmatrix} u & v & r \end{bmatrix}^T$ is the generalised velocity vector in the body-fixed frame, with u, v denoting the linear velocities in surge and sway, and r denoting the angular velocity (yaw rate). The variable $\tau = \begin{bmatrix} \tau_u & \tau_v & \tau_r \end{bmatrix}^T$ represents the controlled input force vector and $\tau_d \in \mathbb{R}^3$ represents the added force vector, which comprises unknown forces acting on the vessel due to various external factors such as wind, currents, forces from the towing system, etc (Fossen & Strand, 1999). The terms M and $R(\psi)$ represent the inertia and rotation matrices respectively, having a 3×3 dimension, with

$$M = \begin{bmatrix} m - X_{\dot{u}} & 0 & 0 \\ 0 & m - Y_{\dot{v}} & mx_G - Y_{\dot{r}} \\ 0 & mx_G - N_{\dot{v}} & I_{z_p} - N_{\dot{r}} \end{bmatrix}, \text{ and,} \tag{2}$$

$$R(\psi) = \begin{bmatrix} \cos(\psi) & -\sin(\psi) & 0 \\ \sin(\psi) & \cos(\psi) & 0 \\ 0 & 0 & 1 \end{bmatrix}. \tag{3}$$

Here, m is the vessel's mass, I_{z_p} is the moment of inertia about the z_p- axis, and, $X_{\dot{u}}$, $Y_{\dot{v}}$, $Y_{\dot{r}}$, $N_{\dot{v}}$ and $N_{\dot{r}}$ are hydrodynamic parameters that account for the added mass. Further, x_G represents the coordinate of the vessel's centre of gravity (COG) along the x_b- axis. The terms $C(\nu)$, $D(\nu)$ are the Coriolis-centripetal and damping matrices, respectively, and are given by

$$C(\nu) = \begin{bmatrix} 0 & 0 & c_{13}(\nu) \\ 0 & 0 & c_{23}(\nu) \\ -c_{13}(\nu) & -c_{23}(\nu) & 0 \end{bmatrix},$$
$$D(\nu) = \begin{bmatrix} d_{11}(\nu) & 0 & 0 \\ 0 & d_{22}(\nu) & d_{23}(\nu) \\ 0 & d_{32}(\nu) & d_{33}(\nu) \end{bmatrix}, \tag{4}$$

with $c_{13}(\nu) = -m(x_G r + v) + Y_{\dot{v}} v + Y_{\dot{r}} r$, $c_{23}(\nu) = mu - X_{\dot{u}} u$, $d_{11}(\nu) = -X_u - X_{|u|u}|u| - X_{uuu}|u^2|$, $d_{22}(\nu) = -Y_v - Y_{|v|v}|v| - Y_{|r|v}|r|$, $d_{23}(\nu) = -Y_r - Y_{|v|r}|v| - Y_{|r|r}|r|$, $d_{32}(\nu) = -N_v - N_{|v|v}|v| - N_{|r|v}|r|$, and $d_{33}(\nu) = -N_r - N_{|v|r}|v| - N_{|r|r}|r|$. The terms X_u, $X_{|u|u}$, X_{uuu}, Y_v, $Y_{|v|v}$, $Y_{|r|v}$, Y_r, $Y_{|v|r}$, $Y_{|r|r}$, N_v, $N_{|v|v}$, $N_{|r|v}$, N_r, $N_{|v|r}$ and $N_{|r|r}$, are the hydrodynamic parameters that account for the damping forces within the second-order modulus model representation (Fedyaevsky & Sobolev, 1964; Skjetne et al., 2004).

2.2. Thrusters modelling

For a twin azimuth-thruster configuration, the controlled input force vector can be defined as

$$\tau = \begin{bmatrix} \tau_u \\ \tau_v \\ \tau_r \end{bmatrix} = \begin{bmatrix} X_{pr,1} + X_{pr,2} \\ Y_{pr,1} + Y_{pr,2} + Y_{\text{bow}} \\ N_{pr,1} + N_{pr,2} + N_{\text{bow}} \end{bmatrix}, \tag{5}$$

where, $X_{pr,i}$, $Y_{pr,i}$ and $N_{pr,i}$ are the generalised force components for the ith thruster, $i \in \{1, 2\}$, such that Marley et al. (2023)

$$\begin{aligned} X_{pr,i} &= F_{t,i}\cos(\delta_{c,i}) - F_{d,i}\cos(\beta_i) - F_{l,i}\sin(\beta_i) \\ Y_{pr,i} &= F_{t,i}\sin(\delta_{c,i}) - F_{d,i}\sin(\beta_i) + F_{l,i}\cos(\beta_i). \\ N_{pr,i} &= x_R Y_{pr,i} - y_{R,i} X_{pr,i} \end{aligned} \tag{6}$$

Here, $F_{t,i}$, $F_{d,i}$ and $F_{l,i}$ represent forces due to the ith thruster acting in the propeller direction, in the relative fluid velocity direction and perpendicular to the relative fluid velocity, respectively. Further, $\delta_{c,i}$ and β_i are the measured or calculated azimuth and flow orientation angles for the ith thruster, respectively. Finally, x_R and $y_{R,i}$ are the longitudinal and lateral coordinates of the thruster's location. The thruster force can be defined using the following quadratic relation:

$$F_{t,i} = C_{t,i}\omega_{c,i}^2, \quad i \in \{1, 2\}, \tag{7}$$

where, the constant $C_{t,i}$ represents the thrust force coefficient and $\omega_{c,i}$ represents the propeller revolutions in rad/s. Furthermore, the force components $F_{d,i}$ and $F_{l,i}$ can be defined as

$$\begin{aligned} F_{d,i} &= 0.5\rho A_R(C_{d,0} + C_{d,1}|\phi_i|)V_i^2 \\ F_{l,i} &= 0.25\rho A_R C_{l,1}\sin(2\phi_i)V_i^2, \quad i \in \{1, 2\}, \end{aligned} \tag{8}$$

where, the terms ρ represents the fluid density, A_R the reference area, $\phi_i = \delta_{c,i} - \beta_i$ is the relative fluid angle of attack and V_i is the total fluid flow velocity. The constants $C_{d,0}, C_{d,1}$ represent the base drag coefficient and its variation w.r.t. ϕ, respectively, whereas constant $C_{l,1}$ represents the variation in the lift coefficient w.r.t. ϕ.

Remark 1. Notably, this work focuses solely on the vessel's high-speed maneuvering; therefore, the bow tunnel thrusters are not employed, resulting in Y_{bow} and N_{bow} having zero values.

The parameters vector $\theta \in \mathbb{R}^{n_\theta}$, $n_\theta = 27$, comprising the parameters in the vessel maneuvering model (Eqs. (1),(5)) to be determined, is given by :

$$\theta = \begin{bmatrix}\theta_1 & \theta_2 & \theta_3\end{bmatrix}^T, \tag{9}$$

where

$$\begin{aligned}\theta_1 &= \begin{bmatrix} I_{z_p} & X_{\dot{u}} & Y_{\dot{v}} & Y_{\dot{r}} & N_{\dot{v}} & N_{\dot{r}} & X_u & X_{|u|u} & X_{uuu}\end{bmatrix},\\ \theta_2 &= \begin{bmatrix} Y_v & Y_{|v|v} & Y_{|r|v} & Y_r & Y_{|v|r} & Y_{|r|r} & N_v & N_{|v|v} & N_{|r|v}\end{bmatrix},\\ \theta_3 &= \begin{bmatrix} N_r & N_{|v|r} & N_{|r|r} & C_{t,1} & C_{t,2} & C_{l,1} & C_{d,0} & C_{d,1} & A_R\end{bmatrix}.\end{aligned} \tag{10}$$

The initial values and bounds for these parameters are determined using empirical formulas, standardised full-scale tests, such as bollard-pull tests, and/or expert knowledge.

The objective of this work is to estimate the aforementioned parameters of a 3-DOF nonlinear maneuvering model using the SMI method and to provide their guaranteed bounds. The proposed method is described in detail in the following section.

3. Set-membership identification (SMI)

SMI enables the identification of unknown system parameters under the assumption of bounded noise and disturbances, thereby avoiding the need for a stochastic treatment for these uncertainties. It requires that the system is linear in the parameters of interest, even if the maneuvering model given by Eq. (1) and the thruster model given by Eqs. (5), (6) are inherently nonlinear with respect to the system states and control inputs. The nonlinear entry of these parameters into the system dynamics also makes the system identification task difficult, as it leads to a nonconvex objective function. This can further lead to the optimisation solver converging to a local minima. Consequently, the identified parameters may not accurately represent the true underlying vessel dynamics. To address these issues, the model is transformed and discretised to obtain a discrete-time linear-in-parameters (DT-LIP) model, given by

$$x(k+1) = G(x(k), u(k))\xi \tag{11a}$$

$$y(k) = x(k) + n(k), \tag{11b}$$

where $G \in \mathbb{R}^{n \times n_\xi}$ denotes a nonlinear basis function in states $x(k) \in \mathbb{R}^n$ and controlled inputs $u(k) \in \mathbb{R}^p$, with $n = 6$ and $p = 4$, respectively, and $y(k)$ is the output, which is a function of $x(k)$ and the measurement noise $n(k)$. The vessel's states $x(k)$ and the controlled inputs $u(k)$ are respectively defined by

$$\begin{aligned}x(k) &= \begin{bmatrix}\eta(k) & \nu(k)\end{bmatrix}^T\\ u(k) &= \begin{bmatrix}\delta_{c,1}(k) & \delta_{c,2}(k) & \omega_{c,1}(k) & \omega_{c,2}(k)\end{bmatrix}^T.\end{aligned} \tag{12}$$

$\xi \in \mathbb{R}^{n_\xi}$, $n_\xi = 78$, is the transformed parameters vector to be identified (See Appendix A). Note that ξ differs from the physical parameters in θ, due to the transformation of the system dynamics into the DT-LIP form, with the transformation function represented by $f : \mathbb{R}^{n_\theta} \to \mathbb{R}^{n_\xi}$. Carrying out this transformation involves formulating ξ by separating the unknown parameters from the known states and inputs and vectorising them, and obtaining G by converting the original nonlinear function in Eq. (1) into a block-matrix form (see, for e.g., Khosla & Kanade, 1985; Martinsen et al., 2020). This transformation is straightforward but omitted for brevity.

The bounded noise assumption can be stated as follows:

Assumption 1. The noise is unknown and bounded by a known upper and lower bound, i.e.,

$$|n(k)| \le \bar{n} \Leftrightarrow n(k) \in \mathcal{N}(k) = \{n(k) \in \mathbb{R}^n, Hn(k) \le h_n\}, \tag{13}$$

where

$$\begin{aligned}H &= \begin{bmatrix} I_n & -I_n\end{bmatrix}^T \in \mathbb{R}^{2n \times n},\\ h_n &= \begin{bmatrix}\underline{n} & \overline{n}\end{bmatrix} \in \mathbb{R}^{2n},\end{aligned} \tag{14}$$

with I_n denoting an identity matrix of dimension n.

The proposed SMI algorithm can be summarised as follows: Firstly, a data-driven parameter set (DDPS), $\Delta(k) \subseteq \mathbb{R}^{n_\xi}$ must be computed, using the DT-LIP description of the system dynamics (Eq. 11), the noise bound (Eq. 13) and the input-output measurements. The input-output measurements could correspond to logged data or real-time measurements, depending on whether the identification is offline or online. Next, the FPS, $\Pi(k) \subseteq \mathbb{R}^{n_\xi}$, is computed, using the DDPS and the previous estimate of the FPS $\Pi(k-1)$. A parameter estimate $\theta^\star$ is obtained by solving a QP over $\bar{\Pi}(k)$, using the DDPS as a constraint. The QP is formulated in terms of the original parameter vector θ instead of the transformed parameter vector ξ, to avoid the need for a nonlinear transformation to invert the system dynamics. Finally, the parameter bounds are obtained by solving a linear program for minimisation/maximisation over the DDPS polytope. In the case of online identification, both the optimal parameter vector estimate and the bounds must be computed at each iteration. The steps to compute the DDPS are described in the next section.

3.1. Data-driven parameter set (DDPS) computation

For the DT-LIP system represented by Eq. (11), the DDPS refers to the set of all parameters that is consistent with the model structure, measurement data and the noise and disturbance bounds at each time step k. The DDPS can be approximated as a polytope computed by firstly combining the equations (11a), (11b), such that

$$y(k+1) = \mathfrak{g}(k) + n(k+1), \tag{15}$$

where the term $\mathfrak{g}(k) \in \mathbb{R}^n$ is given by

$$\mathfrak{g}(k) = G(y(k) - n(k), u(k))\xi, \tag{16}$$

and depends on the output $y(k)$ and the control input $u(k)$, which are known; however, the noise signal $n(k)$ is unknown. Computing the DDPS requires first computing a polytopic bound for this term, which can be obtained via interval analysis. Firstly, a bound on the states can be computed as

$$\begin{aligned}&\underline{x}(k) = y(k) - \bar{n} \le y(k) - n(k) \le y(k) + \bar{n} = \overline{x}(k),\\ \Leftrightarrow\ &x(k) \in [\underline{x}(k), \overline{x}(k)] = [x(k)].\end{aligned} \tag{17}$$

The interval $[x(k)]$ can be updated online for each new measurement. Using equation (17) and interval arithmetic, a time-varying interval bound for the nonlinear basis function $G(y(k) - n(k), u(k))$ can be further computed as in Tsolakis et al. (2025), such that

$$[\underline{G}(k), \overline{G}(k)] \supseteq G([x(k)], u(k)). \tag{18}$$

As a result, Eq. (18) yields the polytopic bounds given by

$$\begin{aligned}&\mathfrak{g}(k) \in \mathcal{G},\\ &\mathcal{G} = \{\mathfrak{g}(k) \in \mathbb{R}^n | H\mathfrak{g}(k) \le h_g(y(k), u(k))\},\end{aligned} \tag{19}$$

where the upper-bound $h_g(y(k), u(k)) \in \mathbb{R}^{2n}$ is calculated using

$$h_g(y(k), u(k)) = \begin{bmatrix}\Delta y(k) + G_r(k)\bar{\xi}\\ -\Delta y(k) + G_r(k)\bar{\xi}\end{bmatrix}. \tag{20}$$

Here, $\Delta y(k)$ is the one-step difference equal to $(y(k+1) - y(k))$, $G_r(k)$ is the radius of the interval matrix $G([x(k)], u(k))$ and $\bar{\xi}$ is a component-wise upper bound vector for ξ. Since the inequalities in (13) and (19) are pre-multiplied by the matrix H, these can be added together, resulting in the following inequality

$$H(\mathfrak{g}(k) + n(k+1)) \le h_g(y(k), u(k)) + h_n. \tag{21}$$

Note that to obtain the above inequality, the noise bound in (13) is shifted forward by one time step. Finally, substituting the relations in (16) and (13) into the LHS of the above equation results in the DDPS given by

$$\begin{aligned}\Delta(k) = \big\{&\xi \in \mathbb{R}^{n_\xi} | HG([x(k)], u(k))\xi \le\\ &h_g(y(k), u(k)) + 2h_n\big\}.\end{aligned} \tag{22}$$

The above equation can be rewritten in a simplified form as

$$\Delta(k) = \{\xi \in \mathbb{R}^{n_\xi} | H_\Delta(k)\xi \leq h_\Delta(k)\}, \tag{23}$$

where $H_\Delta(k) = HG([x(k)], u(k)) \in \mathbb{R}^{2n \times n_\xi}$ and $h_\Delta(k) = h_g(y(k), u(k)) + 2h_n \in \mathbb{R}^{2n}$.

To ensure that the physical parameters can be directly obtained from the parameter identification procedure, the DDPS must be reformulated in terms of the physical parameter vector θ. To carry out this re-formulation, firstly, the nonlinear mapping from the physical parameters to the transformed parameters is linearised as

$$\xi = \xi_0 + J(\delta\theta), \tag{24}$$

where ξ_0 is the initial transformed parameter vector computed by using the initial parameter vector θ_0, and $J = \partial\xi/\partial\theta|_{\theta_0} \in \mathbb{R}^{n_\xi \times n_\theta}$ is the Jacobian computed by finite differences. Rewriting Eq. (22) using the relation in Eq. (24) results in

$$\begin{aligned}\Delta_\theta(k) = &\{\delta\theta \in \mathbb{R}^{n_\theta} | HG([x(k)], u(k))J\delta\theta \leq \\ &-HG([x(k)], u(k))\xi_0 + h_g(y(k), u(k)) + 2h_n\},\end{aligned} \tag{25}$$

which can be rewritten in a simplified form as

$$\Delta_\theta(k) = \{\delta\theta \in \mathbb{R}^{n_\theta} | H_{\Delta_\theta}(k)\delta\theta \leq h_{\Delta_\theta}(k)\}, \tag{26}$$

where $H_{\Delta_\theta}(k) = HG([x(k)], u(k))J \in \mathbb{R}^{2n \times n_\theta}$ and $h_{\Delta_\theta}(k) = -HG([x(k)], u(k))\xi_0 + h_g(y(k), u(k)) + 2h_n \in \mathbb{R}^{2n}$.

3.2. Feasible parameter set computation

The set of all feasible parameters must be computed by recursively updating it using the DDPS, starting from an initial bounded parameter estimate. For the transformed parameters vector ξ, it can be represented using polytopes as

$$\Pi(k) = \{\xi \in \mathbb{R}^{n_\xi} | H_\xi(k)\xi \leq h_\xi(k)\}, \tag{27}$$

where $H_\xi(k) \in \mathbb{R}^{2n_\xi \times n_\xi}$ and $h_\xi(k) \in \mathbb{R}^{2n_\xi}$. Starting from an initial estimate of $H_\xi(0) = \begin{bmatrix} I_{n_\xi} & -I_{n_\xi} \end{bmatrix}^T$ and $h_\xi(0) = \begin{bmatrix} \bar{\xi} & -\underline{\xi} \end{bmatrix}^T$, the FPS update at each time step k is performed such that

$$\Pi(k) = \Pi(k-1) \cap \Delta(k), \forall k = 1, \dots, N. \tag{28}$$

This intersection of the two polytopic sets results in a new set defined by the inequality in (27), with the new pair $(H_\xi(k), h_\xi(k))$ given by

$$H_\xi(k) = \begin{bmatrix} H_\xi(k-1) \\ H_\Delta(k) \end{bmatrix}, \; h_\xi(k) = \begin{bmatrix} h_\xi(k-1) \\ h_\Delta(k) \end{bmatrix}. \tag{29}$$

As new measurements are incorporated, the polytope can quickly explode in size and must be kept bounded to avoid computational burden.

The parameter identification problem is formulated as a QP in the physical parameter increment vector given by $\delta\theta \in \mathbb{R}^{n_\theta}$, around an initial anchor θ_0. Defining $\Phi = H_\xi(N)$ and $\mu = h_\xi(N)$ as the final stacked pair representing the FPS at the Nth time step, the constrained QP can be stated as the following minimisation problem

$$\min_{\delta\theta} \frac{1}{2}\|\Phi(\xi_0 + J(\delta\theta)) - \mu\|_2^2 + \frac{\lambda}{2}\|\delta\theta\|_2^2 \tag{30a}$$

$$\text{s.t. } \underline{\theta} \leq \theta_0 + \delta\theta \leq \bar{\theta}, \tag{30b}$$

$$H_{\Delta_\theta}\delta\theta \leq h_{\Delta_\theta}. \tag{30c}$$

The variable λ represents the regularisation factor that prevents overfitting. Further, the Eq. (30b) represents a box constraint on the physical parameters. The inequality constraint (30c) enforces the DDPS, where $H_{\Delta_\theta}, h_{\Delta_\theta}$ denote a stacked pair obtained by vertical concatenation, i.e.,

$$\begin{aligned} H_{\Delta_\theta} &= \begin{bmatrix} H_{\Delta_\theta}(1) & \dots H_{\Delta_\theta}(N-1) \end{bmatrix}^T \in \mathbb{R}^{2n(N-1) \times n_\theta}, \\ h_{\Delta_\theta} &= \begin{bmatrix} h_{\Delta_\theta}(1) & \dots h_{\Delta_\theta}(N-1) \end{bmatrix}^T \in \mathbb{R}^{2n(N-1)}, \end{aligned} \tag{31}$$

leading to the compact DDPS representation in $\delta\theta$ given by

$$\Delta_\theta = \{\delta\theta \in \mathbb{R}^{n_\theta} | H_{\Delta_\theta}\delta\theta \leq h_{\Delta_\theta}\}. \tag{32}$$

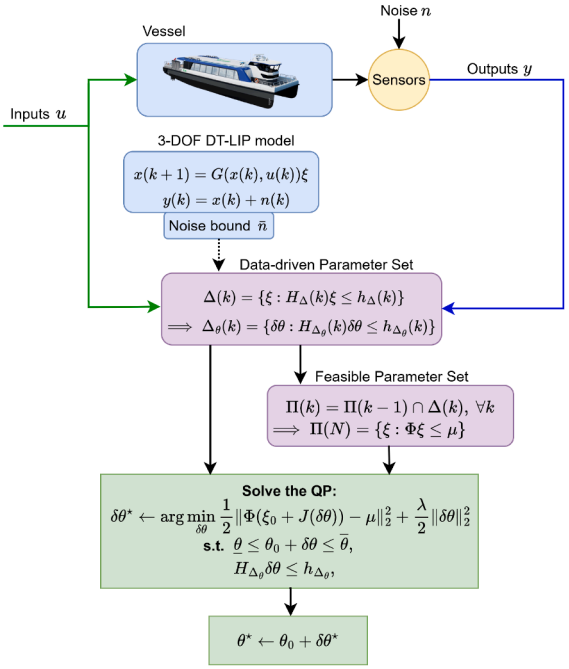

Fig. 2. Architecture of the proposed SMI method.

Table 2
Parameters related to the Damen Waterbus 2907 shuttle.

Parameter	Description	Value	Unit
L_{oa}	Overall length	28.65	m
b	Beam	7.50	m
m	Mass	45000	kg
x_R	Thruster's x-coordinate	−12	m
$y_{R,i}$	Thruster's y-coordinate	± 3.175	m

The resulting solution, $\delta\theta^\star$, is the smallest parameter increment consistent with both the measured input-output data and the FPS. The identified optimal parameters vector is given by

$$\theta^\star = \theta_0 + \delta\theta^\star. \tag{33}$$

Using the above relation, the parameter bounds can also be directly inferred by solving a componentwise min/max problem over the compact DDPS polytope, such that

$$\begin{aligned} \underline{\theta}_i^\star &= \theta_{0,i} + \min_{\delta\theta \in \Delta_\theta} \delta\theta_i \\ \bar{\theta}_i^\star &= \theta_{0,i} + \max_{\delta\theta \in \Delta_\theta} \delta\theta_i, \end{aligned} \tag{34}$$

with $\underline{\theta}_i$ and $\bar{\theta}_i$ denoting the lower and upper bounds for the ith parameter, respectively, for all $i \in \{1, \dots, n_\theta\}$. The overall architecture of the SMI method is illustrated in Fig. 2.

4. System identification: Damen Waterbus 2907 vessel

In this section, the validation results of the proposed method are presented, applied to the Waterbus 2907, a hybrid (diesel and battery) powered water shuttle designed by Damen Shipyards (Damen, 2025), equipped with two azimuth thrusters and two bow thrusters (See Fig. 3). Its main parameters, related to its dimensions and mass, are mentioned in Table 2. The vessel's maneuvering model is identified using logged data, including sensor measurements from the onboard global navigation satellite system (GNSS) and inertial navigation system (INS), as well as the propulsion system, during various maneuvers performed on the Merwede River. The controlled inputs correspond to the azimuth thrusters' angles and revolution speeds, whereas the bow thrusters are not employed, as only high-speed maneuvers are considered.

Table 3
The measurement noise bounds.

Element	Value	Unit	Element	Value	Unit
$\bar{n}(1)$	2	m	$\bar{n}(4)$	0.5	m/s
$\bar{n}(2)$	2	m	$\bar{n}(5)$	0.5	m/s
$\bar{n}(3)$	0.05	rad	$\bar{n}(6)$	0.05	rad/s

Fig. 3. The Waterbus 2907 vessel (Courtesy: Damen shipyards).

The data correspond to tests performed at full speed, including the zig-zag tests (at thruster angles of $+20/-20$, $+10/-10$, and $+5/-5$ degrees) and the turning test, and comprise a total of 3101 data points collected at a sampling rate of 10 Hz. As a result, the total dataset size and the sampling time are $N_{\text{total}} = 3101$ and $T_s = 0.1$ s, respectively. These tests provide sufficient persistence of excitation for the input signals, enabling reliable parameter identification for the given speed profile. The GNSS measurements are collected with real-time kinematic (RTK) positioning enabled, providing centimeter-level precision. Furthermore, the onboard INS provides filtered velocity measurements by fusing raw data from GNSS and IMU sensors. The tests were performed in calm waters, with water currents estimated at 3 km/h along the direction of the river. Further, wind speeds corresponding to a Beaufort Number of 2 were observed. The noise bound vector $\bar{n}$ is obtained using technical specifications for the onboard sensors, and its elements are given in Table 3.

4.1. Identification procedure

Algorithm 1 summarises the overall system identification procedure using the proposed SMI method. For each maneuvering experiment $j = 1, \dots, n_j$, the inputs $u_j \in \mathbb{R}^{N_j \times 4}$, and the measured outputs $y_j \in \mathbb{R}^{N_j \times 6}$ are employed in the identification procedure, where $N_{\text{total}} = N_j \cdot n_j$. Further, noise bounds $\bar{n} \in \mathbb{R}^n$ and the initial physical parameter bounds $[\underline{\theta}, \overline{\theta}]$ are utilised, based on technical datasheets and expert knowledge. At each trial, an initial guess on the parameters, θ_0, is randomly selected inside the parameter bounds. Using θ_0, a transformed parameter vector ξ_0 is obtained by using the transformation function f. In the for-loop (Lines 9-15), the DDPS and FPS are computed for each data point. The DT-LIP representation (Eq. (11a)) is employed to compute the DDPS, using the relation in Eq. (23) (Lines 10-11). In addition, the DDPS is transformed into $\delta\theta$-space in lines 12-13. Finally, the FPS is computed in Line 14, represented by a polytope defined by the pair $(H_\xi(k), h_\xi(k))$. Starting from an initialisation at the transformed bounds $[\underline{\xi}, \overline{\xi}]^T$, it is updated by intersecting it with the DDPS $\Delta(k)$, defined by the pair $(H_\Delta(k), h_\Delta(k))$.

The compact DDPS polytope, represented by the pair $(H_{\Delta_\theta}, h_{\Delta_\theta})$, is obtained by vertically stacking the pairs obtained for each time step. The QP is formulated with respect to $\delta\theta$, to obtain the optimal $\delta\theta^\star$ value (Lines 18-19). Finally, the optimal physical parameter vector $\theta^\star$, and the optimal parameter bounds are obtained. For each experiment, the estimated states can be obtained by simulating the model using the optimal parameter vector $\theta^\star$.

It is noteworthy that Algorithm 1 can also be implemented for online parameter updating, since the DDPS and FPS are recursively updated. However, computational burden in real-time applications must be reduced, particularly for the intersection operation described by Eqs. (28) and (29). Many approaches have been suggested in the literature to address this issue, for example, outer-approximating the FPS at each iteration using predefined normal directions (see Tsolakis et al., 2025).

Algorithm 1 The proposed SMI algorithm.

Input: $\{(u_j(k), y_j(k))\}_{j=1}^{n_j}$ for $k = \{1, \dots, N_j\}$
Parameters: sample time T_s, noise bound $\bar{n} \in \mathbb{R}^n$, initial parameter bounds $\theta \in [\underline{\theta}, \overline{\theta}]$
Output: Optimal parameters per-experiment $\theta_j^\star$, Bounds $[\underline{\theta}_j^\star, \bar{\theta}_j^\star]$

1: **for** $j = 1$ **to** n_j **do**
2: succ $\leftarrow 0$
3: **while** succ $< N_{\text{starts}}$ **do**
4: $h_n \leftarrow \begin{bmatrix} \underline{n} & \bar{n} \end{bmatrix}$
5: $\theta_0 \sim \mathcal{U}([\underline{\theta}, \overline{\theta}])$, $\xi_0 \leftarrow f(\theta_0)$ ▷ random restart
6: $J \leftarrow \partial\xi/\partial\theta|_{\theta_0}$ ▷ Jacobian
7: $\begin{bmatrix} \underline{\xi}, & \overline{\xi} \end{bmatrix} \leftarrow f([\underline{\theta}, \overline{\theta}])$ ▷ transformed bounds
8: $H_\xi(0) \leftarrow \begin{bmatrix} I_{n_\xi} & -I_{n_\xi} \end{bmatrix}^T$, $h_\xi(0) \leftarrow \begin{bmatrix} \underline{\xi} & \overline{\xi} \end{bmatrix}^T$ ▷ initial FPS
9: **for** $k = 1$ **to** $N_j - 1$ **do**
10: $H_\Delta(k) \leftarrow HG([x_j(k)], u_j(k))$
11: $h_\Delta(k) \leftarrow h_g(y_j(k), u_j(k)) + 2h_n$
12: $H_{\Delta_\theta}(k) \leftarrow H_\Delta(k)J$
13: $h_{\Delta_\theta}(k) \leftarrow -HG([x_j(k)], u_j(k))\xi_0 + h_\Delta(k)$
14: $H_\xi(k) \leftarrow \begin{bmatrix} H_\xi(k-1) \\ H_\Delta(k) \end{bmatrix}$, $h_\xi(k) \leftarrow \begin{bmatrix} h_\xi(k-1) \\ h_\Delta(k) \end{bmatrix}$
15: **end for**
16: Build stacked $H_{\Delta_\theta} \in \mathbb{R}^{2n(N_j-1)\times n_\theta}$ and $h_{\Delta_\theta} \in \mathbb{R}^{2n(N_j-1)}$ from $\{H_{\Delta_\theta}(k), h_{\Delta_\theta}(k)\}$
17: $\Phi \leftarrow H_\xi(N) \in \mathbb{R}^{(2n_\xi+2n(N_j-1))\times n_\xi}$ and $\mu \leftarrow h_\xi(N) \in \mathbb{R}^{2n_\xi+2n(N_j-1)}$
18: Solve the QP described in Eq. (30).
19: $\theta_j^\star \leftarrow \theta_0 + \delta\theta_j^\star$
20: $\underline{\theta}_{i,j}^\star = \theta_{0,i} + \min_{\delta\theta\in\Delta_\theta} \delta\theta_i$; $\bar{\theta}_{i,j}^\star = \theta_{0,i} + \max_{\delta\theta\in\Delta_\theta} \delta\theta_i$, for $i \in \{1, \dots, n_\theta\}$
21: succ $\leftarrow$ succ $+ 1$
22: **end while**
23: **end for**

4.2. Identification results

The parameters of the 3-DOF model of the vessel obtained by using Algorithm 1 are summarised in Table 4. These correspond to the inertia- and added-mass-related parameters, the hydrodynamic derivatives, and the actuation-related parameters. The identified parameters are further validated by predicting the vessel's states, as described in the following subsections. The simulations are performed using MATLAB, on a Dell Latitude 7430 with 16 GB RAM and a 1.80 GHz 12th Gen Intel(R) Core(TM) i7-1265U processor.

4.2.1. Validation using simulations

The identified model is further validated by predicting the vessel's linear velocities and yaw rate, and comparing these predictions with the measurements. Fig. 4 shows the controlled inputs, namely the azimuth angles and the propeller revolutions, and the corresponding states predicted using the identified model. The predicted trajectories closely match the measured data, demonstrating that the identified model accurately captures the vessel's dynamic behaviour across diverse maneuvers. The slight offset observed in the sway and yaw velocities is likely due to a combination of two related factors. First, the model assumes still water conditions, i.e., the relative velocity due to currents is not taken into account. However, during the tests, a mild river current was observed (at an estimated speed of 3 km/h), contributing to the vessel's sideslip and yaw moment. Secondly, wind speeds during the tests,

Table 4
Identified parameters of the DAMEN Waterbus 2907 shuttle.

Parameter	I_{z_p}	$X_{\dot{u}}$	$Y_{\dot{v}}$	$Y_{\dot{r}}$	$N_{\dot{v}}$	$N_{\dot{r}}$	X_u	$X_{\|u\|u}$	X_{uuu}
Value	2.7×10^6	−1945.16	−28921.48	−34885.49	−27909.24	−197285.14	−0.00	−642.59	−0.00
Unit	kgm^2	kg	kg	kgm	kgm	kgm^2	kg/s	kg/m	kgs^2/m^2
Parameter	Y_v	$Y_{\|v\|v}$	$Y_{\|r\|v}$	Y_r	$Y_{\|v\|r}$	$Y_{\|r\|r}$	N_v	$N_{\|v\|v}$	$N_{\|r\|v}$
Value	−12.93	−24921.71	−95742.81	256.50	−929504.91	496954.14	444.81	213501.59	−70223.26
Unit	kg/s	kg/m	kg	kgm	kg	kgm/rad	kgm	kgm	kgm^2
Parameter	N_r	$N_{\|v\|r}$	$N_{\|r\|r}$	$C_{t,1}$	$C_{t,2}$	$C_{l,1}$	$C_{d,0}$	$C_{d,1}$	A_R
Value	−0.19	−355262.69	−37454.15	1.25	1.06	0.1	0.1	0.1	8
Unit	kg m^2/s	kgm^2	kgm^2	Ns^2/rad^2	Ns^2/rad^2	-/rad	–	-/rad	m^2

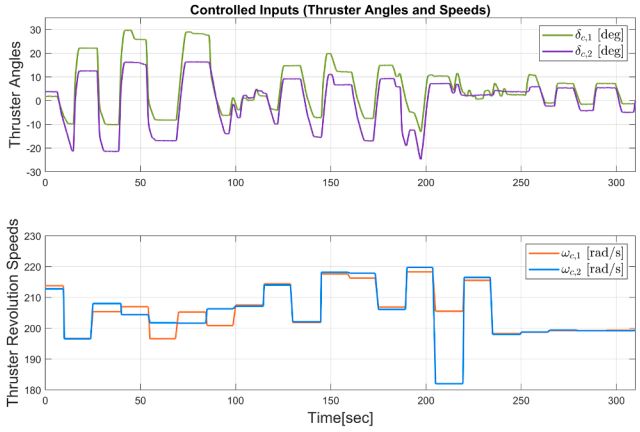

(a) Controlled inputs including the angles and revolution speeds for the port-side and starboard thrusters, respectively.

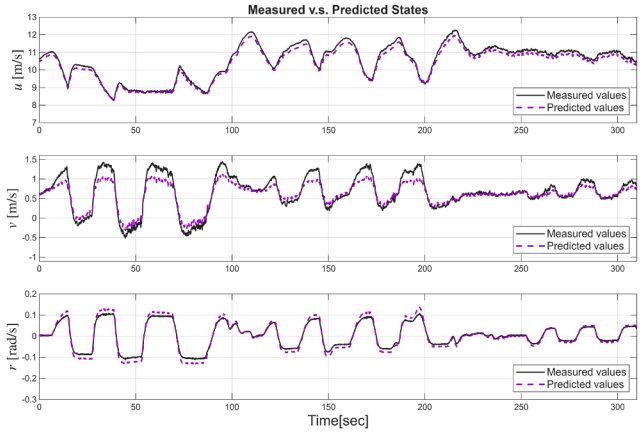

(b) Comparison between the vessel's measured linear and angular velocities and the corresponding predicted values.

Fig. 4. The controlled inputs and the corresponding outputs, including the measured and predicted states. The predicted states are obtained using the vessel's identified model.

although small in magnitude (estimated to be between 4-6 knots), can lead to time-varying sway forces and yaw moments, with their signs depending on the vessel's heading. To eliminate these errors and achieve higher prediction accuracy, incorporating a disturbance model for wind and current or including bounded disturbances in the DDPS can be beneficial.

Subsequently, the prediction accuracy and computational times are quantitatively evaluated using two performance metrics. Firstly, the percentage fit metric (J_{fit}) is calculated for each state as

$$J_{\text{fit}} = \max\left(0, 100\left(1 - \frac{\|y_x - \hat{x}\|}{\max(y_{\text{ref}}, \epsilon)}\right)\right), \tag{35}$$

where y_x and $\hat{x}$ represent the measured and predicted states, respectively, y_{ref} is the reference value, equal to the initial measurement, and ϵ is a scalar having a small value. Next, the computational time metric J_{comp} is calculated to underline the feasibility of real-time application of the identification procedure. This metric is calculated as

$$J_{\text{comp}} = \frac{t_{\text{CPU}}}{N_{\text{total}}}, \tag{36}$$

where t_{CPU} is calculated by using MATLAB's `tic` and `toc` functions, at the beginning and end of the identification algorithm, and N_{total} is the total size of the dataset. The average values obtained for the aforementioned metrics are presented in Table 5 for each test maneuver. Across all maneuvers, the proposed SMI algorithm achieves a higher average J_{fit} value than MATLAB's `nlgreyest` algorithm, further confirming its accuracy and generalizability. In addition, the average J_{comp} value is at least one order of magnitude lower, supporting the case for online implementation of the SMI algorithm.

4.2.2. *Optimal parameter bounds*

For each identified parameter, optimal bounds are computed by solving the pair of linear programs in Eq. (34) over the DDPS polytope. The resulting intervals are mentioned in Table 6, and visualised in the box plot as shown in Fig. 5. Most parameters exhibit narrow intervals, indicating that they are tied to directions well excited by the data. The intervals are expected to shrink as more informative data are added to the DDPS set and to widen when the noise bounds are expanded. Importantly, the intervals remain non-empty and physically interpretable across all runs, indicating that the data are free of anomalies.

4.3. *Validation using synthetic data*

Validation using synthetic data provides a controlled benchmark for evaluating the proposed algorithm's accuracy. In this setting, the synthetic dataset is generated using a known model structure and parameter set, allowing direct comparison between the identified and true parameters. This enables the assessment of the algorithm's ability to accurately recover the physical parameters under idealised and controlled noise conditions. The synthetic data comprises controlled inputs and outputs for various simulated maneuvers of the vessel. Sensor noise is simulated using the bounds described in Table 3. The resulting magnitudes of the identified parameters using synthetic data are shown in Fig. 6. As shown, the identified parameters are plotted for three scenarios: noiseless synthetic data (yellow markers), noisy synthetic data (blue markers), and real-world experimental data (green markers). The parameters identified from real-world data also serve as the ground truth. It can be observed that the identified parameters lie within the same range as the ground truth and within the previously obtained parameter bounds (Table 6). Importantly, the parameter sign consistency is maintained across

Table 5
Comparison between the average values of the percentage fit and computational time metrics corresponding to each test maneuver.

	Zig-zag (−20/20)	Zig-zag (−10/10)	Zig-zag (−5/5)	Turning
	Average J_{fit} value			
MATLAB's `nlgreyest`	81.45	76.11	61.54	81.49
SMI (Algorithm 1)	**86.04**	**83.59**	**88.08**	**86.49**
	Average J_{comp} value [sec]			
MATLAB's `nlgreyest`	0.0184	0.0228	0.0156	0.0273
SMI (Algorithm 1)	**0.0023**	**0.0030**	**0.0008**	**0.0029**

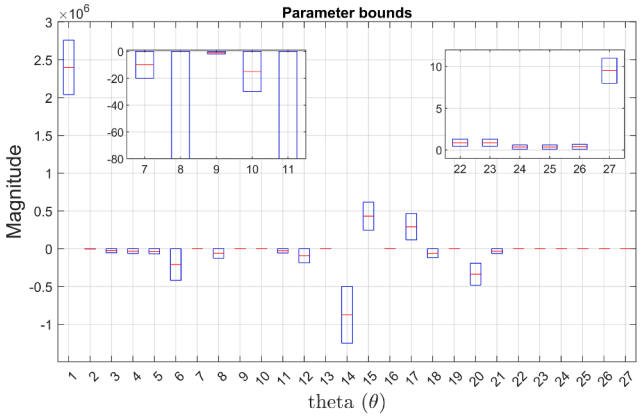

Fig. 5. Box plot showcasing the lower and upper bounds on the parameters' magnitudes. The parameters are arranged in the x-axis according to the corresponding element's index in Eq. (9).

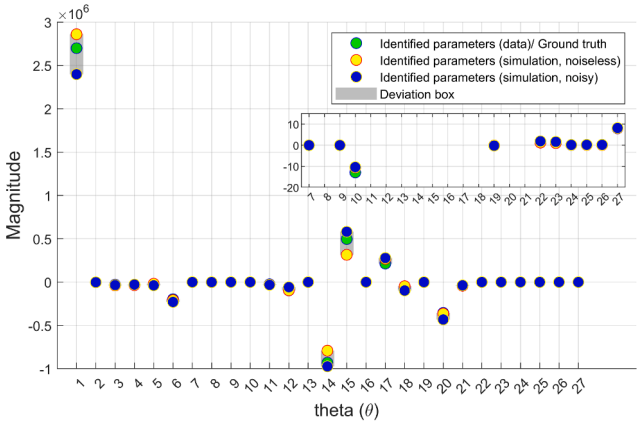

Fig. 6. Comparison of various parameter magnitudes identified from simulations and real data, along with their ground truth values.

Table 6
The estimated lower and upper bound values obtained for the identified parameters.

Par.	L.B.	U.B.	Par.	L.B.	U.B.
I_{z_p}	2.04×10^6	2.76×10^6	$Y_{\|r\|r}$	246031.5	615078.75
$X_{\dot{u}}$	−4120	0	N_v	0	790
$Y_{\dot{v}}$	−54370	0	$N_{\|v\|v}$	115993	463972
Y_r	−63150	0	$N_{\|r\|v}$	−120462	0
$N_{\dot{v}}$	−68942	0	N_r	−0.45	0
$N_{\dot{r}}$	−418910	0	$N_{\|v\|r}$	−481073.75	−192429.5
X_u	−20	0	$N_{\|r\|r}$	−63174	0
$X_{\|u\|u}$	−128706.92	0	$C_{t,1}$	0.44	1.31
X_{uuu}	−2.00	0	$C_{t,2}$	0.44	1.31
Y_v	−30.00	0	$C_{l,1}$	0.1	0.6
$Y_{\|v\|v}$	−56668	0	$C_{d,0}$	0.1	0.6
$Y_{\|r\|v}$	−187748	0	$C_{d,1}$	0.1	0.7
Y_r	0	462	A_R	8	11
$Y_{\|v\|r}$	−1251352.5	−500541			

all cases. This indicates that the identification method generalises well beyond idealised simulations and yields physically reliable results.

4.4. Sensitivity analysis

Next, the identified model's sensitivity is evaluated by propagating parameter uncertainty through the predicted vessel states. This helps determine the impact of parameter variation on prediction accuracy. Firstly, a total of 500 parameter vector samples $\theta^{(s)} \in \mathbb{R}^{n_\theta}$ were uniformly generated within the obtained parameter bounds, such that,

$$\underline{\theta}_i^\star \le \theta_i^{(s)} \le \bar{\theta}_i^\star, \quad i \in \{1, \dots, n_\theta\}. \tag{37}$$

For each sample, the nonlinear state update is performed using the available control inputs, resulting in multiple predicted trajectories over the full horizon (N_{total}). Further, prediction uncertainty bands are obtained by calculating the minimum and maximum values at each time instant across samples. The resulting plots, including predictions using the nominal and median parameter vectors ($\theta^\star, \bar{\theta}$, respectively), the prediction band for each velocity component, are compared with the measured values, and visualised in Fig. 7. As observed, a tight prediction uncertainty band is obtained that closely follows the measurements, with the nominal and median parameter vectors offering similar prediction accuracies within the band.

To quantify model accuracy for each sampled parameter vector $\theta^{(s)}$, a root mean squared error (RMSE)-based performance metric J_{RMSE} is defined, and is given by

$$J_{\text{RMSE}}(\theta^{(s)}) = \sum_{k=1}^{N_{\text{total}}} (y_x(k) - \hat{x}(\theta^{(s)}, k))^2, \tag{38}$$

where $y_x(k)$ represents the measured state at the kth time-instant, and $\hat{x}(\theta^{(s)}, k)$ represents the predicted state value at the kth time-instant obtained using sample $\theta^{(s)}$. To determine the parameter-wise sensitivity and the most crucial parameters for predictive accuracy, the Spearman rank correlation between each parameter θ_i^s and J_{RMSE} is computed across the samples. The Spearman coefficient, denoted by $\rho_s(\theta_i, J_{\text{RMSE}})$, correlates the ranks of the sampled values, and returns a correlation factor $\rho \in [-1, 1]$, with a ±1 indicating strong correlation between the parameter θ_i and J_{RMSE}, whereas values close to zero indicating small correlation over the range of samples (Corder & Foreman, 2014).

Fig. 8 plots the bar graphs for all parameters with their corresponding Spearman coefficients arranged in a descending order of their magnitudes. Notably, the moment of inertia parameter I_{z_p}, the yaw cross-coupling resistance parameter $N_{|v|r}$, and the second-order surge resistance parameter $X_{|u|u}$ obtain the highest values, implying that their variation within the parameter bound range is consistently related to the changes in the prediction quality. Specifically, the coefficients for I_{z_p}

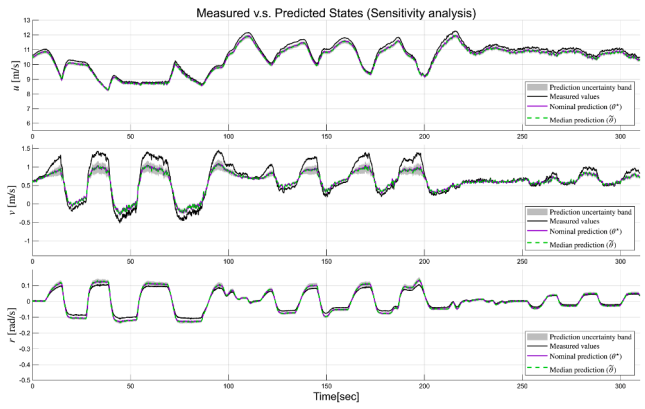

Fig. 7. Plots of the vessel's measured linear and angular velocities and the corresponding predicted values obtained at the nominal (optimal) parameter ($\theta^\star$), the median parameter ($\tilde{\theta}$) in the parameter bounds, and the uncertainty band representing the minimum and maximum state predictions.

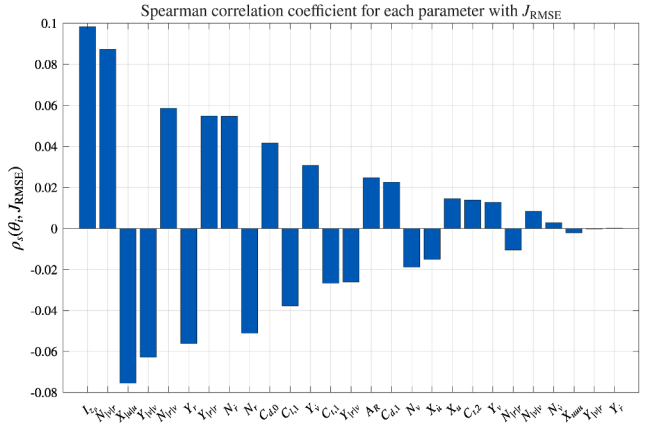

Fig. 8. Spearman rank correlation coefficient for each parameter across the samples, with the prediction error metric J_{RMSE}.

and $N_{|v|r}$ are positive, indicating that increasing their magnitudes tends to produce higher J_{RMSE} values, as the yaw response becomes more distorted. By contrast, for $X_{|u|u}$, the negative coefficient value indicates that increasing its magnitude will reduce J_{RMSE} by improving the surge dynamics. On the other hand, the third-order surge resistance parameter X_{uuu}, as well as the sway resistance parameters $Y_{|v|r}$, $Y_{\dot{r}}$, have the least impact on J_{RMSE}, or their effect is masked by interactions with other parameters. It is also important to note that all coefficients have magnitudes within ± 0.1, implying that none of the parameters dominates the prediction error on its own.

5. Conclusion

This paper proposed an SMI method for parameter identification of a full-scale 3-DOF vessel maneuvering model. The method relies on unknown but bounded descriptions for sensor noise and disturbances to deliver both nominal parameters and their bounds via the solution of convex programs. Validation using data from experimental trials with a full-scale catamaran ferry demonstrated that the proposed method yields parameters with improved state prediction accuracy while requiring less computational time, as compared to MATLAB's built-in grey-box identification method. Specifically, the prediction accuracy improved by up to 26.5% and the computational time reduced by up to one order of magnitude per sample. Furthermore, the identified parameters were consistently obtained within definite bounds across all experimental and synthetic data validation. The obtained bounds facilitate the derivation of explicit guarantees for robustness and safety. Finally, through sensitivity analysis, the impact of parameter variation on the predicted trajectories was evaluated, and the most crucial parameters were identified.

Future work will focus on model identification while including diverse operations, speed profiles, and environmental disturbances, thereby facilitating dock-to-dock autonomy. In addition, online SMI for real-time parameter adaptation can enable robust, adaptive control strategies and is also proposed for future research.

CRediT authorship contribution statement

Abhishek Dhyani: Writing – review & editing, Writing – original draft, Visualization, Validation, Software, Resources, Methodology, Investigation, Formal analysis, Data curation, Conceptualization; **Anastasios Tsolakis:** Writing – review & editing, Software, Methodology, Investigation; **Kasper van der El:** Writing – review & editing, Supervision, Resources, Project administration, Funding acquisition, Data curation; **Rudy R. Negenborn:** Writing – review & editing, Supervision, Project administration, Funding acquisition; **Vasso Reppa:** Writing – review & editing, Supervision, Project administration, Funding acquisition.

Declaration of competing interest

No conflict of interest.

Appendix A. Transformed parameter vector

$$\xi = \begin{bmatrix} \xi_1 & \xi_2 & \xi_3 \end{bmatrix}^T, \tag{39}$$

with

$$\xi_1 = \frac{1}{(X_{\dot{u}} - m)} \begin{bmatrix} -X_u \\ 0 \\ 0 \\ 0 \\ 0 \\ (Y_{\dot{v}} - m) \\ -X_{|u|u} \\ 0 \\ 0 \\ 0 \\ 0 \\ (Y_{\dot{r}} - mx_G) \\ -X_{uuu} \\ -C_{t,1} \\ -C_{t,2} \\ -a_2 \\ -a_2 \\ -a_3 \\ -a_3 \\ -a_4 \\ -a_4 \\ 0 \\ 0 \\ 0 \\ 0 \\ 0 \end{bmatrix}^T,$$

$$\xi_2 = \frac{1}{a_5} \begin{bmatrix} 0 \\ -(I_{z_p} Y_v - N_{\dot{r}} Y_{\dot{v}} + N_v Y_{\dot{r}} - N_v m x_G) \\ -(I_{z_p} Y_r + N_r Y_{\dot{r}} - N_{\dot{r}} Y_r - N_r m x_G) \\ ((X_{\dot{u}} - Y_{\dot{v}})(Y_{\dot{r}} - m x_G)) \\ -(I_{z_p} X_{\dot{u}} + m^2 x_G^2 - N_{\dot{r}} X_{\dot{u}} - I_{z_p} m + N_{\dot{r}} m + Y_{\dot{r}}^2 - 2 Y_{\dot{r}} m x_G) \\ 0 \\ 0 \\ -(I_{z_p} Y_{vv} - N_{\dot{r}} Y_{v|v} + N_{vv} Y_{\dot{r}} - N_{vv} m x_G) \\ -(I_{z_p} Y_{rr} - N_{\dot{r}} Y_{rr} + N_{rr} Y_{\dot{r}} - N_{rr} m x_G) \\ -(I_{z_p} Y_{rv} - N_{\dot{r}} Y_{rv} + N_{rv} Y_{\dot{r}} - N_{rv} m x_G) \\ -(I_{z_p} Y_{vr} - N_{\dot{r}} Y_{v|r} + N_{vr} Y_{\dot{r}} - N_{vr} m x_G) \\ 0 \\ 0 \\ (C_{t,1} Y_r (Y_{\dot{r}} - m x_G)) \\ (C_{t,2} Y_r (Y_{\dot{r}} - m x_G)) \\ (a_2 Y_r (Y_{\dot{r}} - m x_G)) \\ -(a_2 Y_r (Y_{\dot{r}} - m x_G)) \\ (a_3 Y_r (Y_{\dot{r}} - m x_G)) \\ -(a_3 Y_r (Y_{\dot{r}} - m x_G)) \\ (a_4 Y_r (Y_{\dot{r}} - m x_G)) \\ -(a_4 Y_r (Y_{\dot{r}} - m x_G)) \\ -(C_{t,1}(a_7)) \\ -(C_{t,2}(a_7)) \\ -(a_2(a_7)) \\ -(a_3(a_7)) \\ -(a_4(a_7)) \end{bmatrix}^T,$$

$$\xi_3 = \frac{1}{a_5} \begin{bmatrix} 0 \\ (N_v Y_{\dot{v}} - N_{\dot{v}} Y_v - N_v m + Y_v m x_G) \\ (N_r Y_{\dot{v}} - N_{\dot{v}} Y_r - N_r m + Y_r m x_G) \\ -((X_{\dot{u}} - Y_{\dot{v}})(Y_{\dot{v}} - m)) \\ -(N_{\dot{v}} X_{\dot{u}} - Y_{\dot{r}} Y_{\dot{v}} - N_{\dot{v}} m + Y_{\dot{r}} m - X_{\dot{u}} m x_G + Y_{\dot{v}} m x_G) \\ 0 \\ 0 \\ -(N_{\dot{v}} Y_{vv} - N_{vv} Y_{\dot{v}} + N_{vv} m - Y_{vv} m x_G) \\ (N_{rr} Y_{\dot{v}} - N_{\dot{v}} Y_{rr} - N_{rr} m + Y_{rr} m x_G) \\ (N_{rv} Y_{\dot{v}} - N_{\dot{v}} Y_{rv} - N_{rv} m + Y_{rv} m x_G) \\ -(N_{\dot{v}} Y_{vr} - N_{vr} Y_{\dot{v}} + N_{vr} m - Y_{vr} m x_G) \\ 0 \\ 0 \\ -(C_{t,1} Y_r (Y_{\dot{v}} - m)) \\ -(C_{t,2} Y_r (Y_{\dot{v}} - m)) \\ -(a_2 Y_r (Y_{\dot{v}} - m)) \\ (a_2 Y_r (Y_{\dot{v}} - m)) \\ -(a_3 Y_r (Y_{\dot{v}} - m)) \\ (a_3 Y_r (Y_{\dot{v}} - m)) \\ -(a_4 Y_r (Y_{\dot{v}} - m)) \\ (a_4 Y_r (Y_{\dot{v}} - m)) \\ -(C_{t,1}(a_6)) \\ -(C_{t,2}(a_6)) \\ -(a_2(a_6)) \\ -(a_3(a_6)) \\ -(a_4(a_6)) \end{bmatrix}^T \tag{40}$$

where $a_2 = 0.5\rho A_R C_{d,0}$, $a_3 = 0.5\rho A_R C_{d,1}$, $a_4 = 0.5\rho A_R (0.9 C_{l,1})$, $a_5 = I_{z_p} Y_{\dot{v}} + m^2 x_G^2 - N_{\dot{r}} Y_{\dot{v}} + N_{\dot{v}} Y_{\dot{r}} - I_{z_p} m + N_{\dot{r}} m - N_{\dot{v}} m x_G - Y_{\dot{r}} m x_G$, $a_6 = N_{\dot{v}} - Y_{\dot{v}} x_R + m x_R - m x_G$, $a_7 = I_{z_p} - N_{\dot{r}} + Y_{\dot{r}} x_R - m x_R x_G$.

References

Alexandersson, M., Mao, W., & Ringsberg, J. W. (2022). System identification of vessel manoeuvring models. *Ocean Engineering*, *266*, 112940.

Birk, L. (2019). ITTC 1978 performance prediction method. John Wiley & Sons, Ltd. Section: 44.

Corder, G. W., & Foreman, D. I. (2014). Nonparametric statistics: A step-by-step approach. John Wiley & Sons.

Damen (2025). Waterbus 2907 hybrid. https://www.damen.com/vessels/ferries/city-ferries/waterbus-2907-hybrid.

Der Kiureghian, A., & Ditlevsen, O. (2009). Aleatory or epistemic? Does it matter? *Structural Safety*, *31*(2), 105–112.

Dhyani, A., van der El, K., Negenborn, R. R., & Reppa, V. (2026). Multiple sensor fault diagnosis for safe navigation of autonomous surface vessels. *Control Engineering Practice*, *168*, 106673.

Dhyani, A., Mojaveri, A. H., Zhang, C., Mahipala, D., Tran, H. A., Zhang, Y.-Y., Luo, Z., & Reppa, V. (2025). AUTOBargeSim: MATLAB® toolbox for the design and analysis of the guidance and control system for autonomous inland vessels. *IFAC-PapersOnLine*, *59*(22), 818–823. 16th IFAC Conference on Control Applications in Marine Systems, Robotics and Vehicles CAMS 2025.

Eriksen, B.-O. H., & Breivik, M. (2017). Modeling, identification and control of high-speed ASVs: Theory and experiments. In *Sensing and control for autonomous vehicles: Applications to land, water and air vehicles* (pp. 407–431). Springer.

Fedyaevsky, K. K., & Sobolev, G. V. (1964). Control and stability in ship design. State Union Shipbuilding Industry Publishing House.

Fossen, T. I., & Strand, J. P. (1999). Passive nonlinear observer design for ships using Lyapunov methods: Full-scale experiments with a supply vessel. *Automatica*, *35*(1), 3–16.

Hahn, T., Damerius, R., & Jeinsch, T. (2021). An identification scheme to determine all off-diagonal elements of added-mass matrix for marine vessels. *IFAC-PapersOnLine*, *54*(16), 175–180.

Hahn, T., Kolewe, B., & Jeinsch, T. (2023). Identification of a maneuvering vessel based on regular operation. *IFAC-PapersOnLine*, *56*(2), 11584–11589.

Khosla, P. K., & Kanade, T. (1985). Parameter identification of robot dynamics. In *1985 24th IEEE conference on decision and control* (pp. 1754–1760). IEEE.

Lorenzen, M., Cannon, M., & Allgöwer, F. (2019). Robust MPC with recursive model update. *Automatica*, *103*, 461–471.

Luo, W. (2016). Parameter identifiability of ship manoeuvring modeling using system identification. *Mathematical Problems in Engineering*, *2016*(1), 8909170.

Marley, M., Skjetne, R., Gil, M., & Krata, P. (2023). Four degree-of-freedom hydrodynamic maneuvering model of a small azipod-actuated ship with application to onboard decision support systems. *IEEE Access*, *11*, 58596–58609.

Martinsen, A. B., Lekkas, A. M., Gros, S., Glomsrud, J. A., & Pedersen, T. A. (2020). Reinforcement learning-based tracking control of USVS in varying operational conditions. *Frontiers in Robotics and AI*, *7*, 32.

Milanese, M., & Vicino, A. (1991). Optimal estimation theory for dynamic systems with set membership uncertainty: An overview. *Automatica*, *27*(6), 997–1009.

Pedersen, A. A. (2019). Optimization based system identification for the milliampere ferry. Master's thesis. NTNU.

Rauh, A., Lahme, M., Rohou, S., Jaulin, L., Dinh, T. N., Raissi, T., & Fnadi, M. (2023). Offline and online use of interval and set-based approaches for control and state estimation: A review of methodological approaches and their application. *Logical Methods in Computer Science*, *21*(4), 11:1–11:34.

Revestido Herrero, E., & Velasco González, F. J. (2012). Two-step identification of nonlinear manoeuvring models of marine vessels. *Ocean Engineering*, *53*, 72–82.

Skjetne, R., Smogeli, Ø. N., & Fossen, T. I. (2004). A nonlinear ship manoeuvering model: Identification and adaptive control with experiments for a model ship. *Modeling, Identification and Control*, *25*(1), 3–27.

Song, C., Zhang, X., & Zhang, G. (2022). Nonlinear Identification for 4-DOF ship maneuvering modeling via full-scale trial data. *IEEE Transactions on Industrial Electronics*, *69*(2), 1829–1835.

Sonnenburg, C. R., & Woolsey, C. A. (2013). Modeling, identification, and control of an unmanned surface vehicle. *Journal of Field Robotics*, *30*(3), 371–398.

Tanaskovic, M., Fagiano, L., Smith, R., & Morari, M. (2014). Adaptive receding horizon control for constrained MIMO systems. *Automatica*, *50*(12), 3019–3029.

Tsolakis, A., Ferranti, L., & Reppa, V. (2025). Set-membership estimation for fault diagnosis of nonlinear systems. In *2025 European control conference (ECC)* (pp. 1143–1150). IEEE.

Wang, T., Li, G., Hatledal, L. I., Skulstad, R., AEsoy, V., & Zhang, H. (2022). Incorporating approximate dynamics into data-driven calibrator: A representative model for ship maneuvering prediction. *IEEE Transactions on Industrial Informatics*, *18*(3), 1781–1789.

Wang, T., Skulstad, R., Kanazawa, M., Li, G., & Zhang, H. (2024). Learning nonlinear dynamics of ocean surface vessel with multistep constraints. *IEEE Transactions on Industrial Informatics*, *20*(9), 10847–10856.

Wu, G., Zhang, J., Li, G., Wang, L., Yu, Q., & Guo, J. (2022). Identification method of nonlinear maneuver model for unmanned surface vehicle from sea trial data based on support vector machine. *Journal of Mechanical Science and Technology*, *36*(8), 4257–4267.

Zhang, C., Dhyani, A., Ringsberg, J. W., Thies, F., Negenborn, R. R., & Reppa, V. (2025). Nonlinear model predictive control for path following of autonomous inland vessels in confined waterways. *Ocean Engineering*, *334*, 121592.

Zhang, X., Meng, Y., Liu, Z., & Zhu, J. (2022). Modified grey wolf optimizer-based support vector regression for ship maneuvering identification with full-scale trial. *Journal of Marine Science and Technology*, *27*(1), 576–588. Number: 1 Publisher: Springer Japan.

Zhang, Y.-Y., Billet, J., & Slaets, P. (2024). Experimental identification of decoupled ship dynamic Models for an autonomous catamaran urban cargo vessel. *IFAC-PapersOnLine*, *58*(20), 229–234. 15th IFAC Conference on Control Applications in Marine Systems, Robotics and Vehicles CAMS 2024.